NMR Structure of Varkud Satellite Ribozyme Stem−Loop V in the Presence of Magnesium Ions and Localization of Metal-Binding Sites[†,‡]

Dean O. Campbell,[§] Patricia Bouchard,[||] Geneviève Desjardins,[||] and Pascale Legault*[,§,||]

Department of Biochemistry and Molecular Biology, University of Georgia, Athens, Georgia 30602, and Département de Biochimie, Université de Montréal, C.P. 6128, Succursale Centre-Ville, Montréal, QC, Canada H3C 3J7

Received April 13, 2006; Revised Manuscript Received July 10, 2006

ABSTRACT: In the *Neurospora* VS ribozyme, magnesium ions facilitate formation of a loop−loop interaction between stem−loops I and V, which is important for recognition and activation of the stem−loop I substrate. Here, we present the high-resolution NMR structure of stem−loop V (SL5) in the presence of Mg^{2+} ($SL5^{Mg}$) and demonstrate that Mg^{2+} induces a conformational change in which the SL5 loop adopts a compact structure with most characteristics of canonical U-turn structures. Divalent cation-binding sites were probed with Mn^{2+}-induced paramagnetic line broadening and intermolecular NOEs to $Co(NH_3)_6^{3+}$. Structural modeling of $Mn(H_2O)_6^{2+}$ in $SL5^{Mg}$ revealed four divalent cation-binding sites in the loop. Sites 1, 3, and 4 are located in the major groove near multiple phosphate groups, whereas site 2 is adjacent to N7 of G697 and N7 of A698 in the minor groove. Cation-binding sites equivalent to sites 1−3 in SL5 are present in other U-turn motifs, and these metal-binding sites may represent a common feature of the U-turn fold. Although magnesium ions affect the loop conformation, they do not significantly change the conformation of residues 697−699 involved in the proposed Watson−Crick base pairs with stem−loop I. In both the presence and the absence of Mg^{2+}, G697, A698, and C699 adopt an A-form structure that exposes their Watson−Crick faces, and this is compatible with their proposed interaction with stem−loop I. In $SL5^{Mg}$, however, U700 becomes exposed on the minor groove face of the loop in the proximity of the bases of G697, A698, and C699, suggesting that the Mg^{2+}-bound conformation of stem−loop V allows additional contacts with stem−loop I. These studies improve our understanding of the role of Mg^{2+} in U-turn structures and in substrate recognition by the VS ribozyme.

Metal ions play an essential role in RNA biochemistry, because they help maintain the structural and functional integrity of RNA. Positively charged metal ions provide the necessary electrostatic stabilization for formation of complex three-dimensional RNA structures where phosphate anions often become closely packed. Localization of metal cations in structures of RNA, such as group I intron ribozymes (*1*−*4*) and ribosomal RNAs (*5*, *6*), has provided examples for the importance of metal ions in stabilizing local structures, as well as in mediating helical packing. In addition, functional and structural studies have implicated cations in the chemical reaction of several ribozymes (for a recent review, see ref *7*; see also refs *2*−*4* and *8*). Magnesium ions (Mg^{2+}) are particularly important because they stabilize a variety of RNA structures and can support catalysis of many ribozymes at physiological concentrations. An ongoing challenge is to unravel the precise role(s) of magnesium ions in the folding of various RNAs and in Mg^{2+}-assisted RNA catalysis (*2*−*4*, *7*−*9*).

The *Neurospora* VS ribozyme is one of the few naturally occuring self-cleaving ribozymes, and it possesses unique primary, secondary, and tertiary structures (for recent reviews, see refs *10* and *11*). The primary activity of this ribozyme is a metal-dependent autolytic cleavage of the VS RNA to produce 5′-OH and 2′,3′-cyclic phosphate termini, which is similar to that of other small catalytic RNAs such as the hammerhead, hairpin, and hepatitis delta virus ribozymes (*12*). The VS ribozyme is also capable of trans cleavage upon incubation of the separately synthesized substrate and catalytic domains (*13*) and, under the right conditions, can perform ligation reactions (*14*, *15*). The secondary structure of the VS ribozyme (Figure 1a) consists of six helical subdomains (I−VI) (Figure 1a). The catalytic domain of the ribozyme is formed by stem−loops II−VI, whereas stem−loop I defines the substrate domain. Phosphodiester bond cleavage occurs at G620 in the internal loop of stem−loop I (Figure 1a). Nucleotide modification data indicate that the A730 loop of stem−loop VI plays an important role in catalysis and likely constitutes the active site of the *Neurospora* VS ribozyme (*16*, *17*). It has been suggested that for cleavage to occur, the stem−loop I substrate must dock into a cleft formed by stem−loops II

[†] This work was supported by a graduate scholarship from the Université de Montréal to P.B., a scholarship from the Fonds Québécois de la Recherche sur la Nature et les Technologies to G.D., National Science Foundation (NSF) Career Award 9984582 and Canadian Institutes for Health Research (CIHR) Grant MOP-64341. P.L. holds a Canada Research Chair in Structural Biology of RNA.

[‡] The structural coordinates for $SL5^{Mg}$ (PDB entry 1YN1) and for $SL5^{Mg}$ with $Mn(H_2O)_6^{2+}$ (PDB entry 1YN2) have been deposited.

* To whom correspondence should be addressed: Département de Biochimie, Université de Montréal, C.P. 6128, Succursale Centre-Ville, Montréal, QC, Canada H3C 3J7. Phone: (514) 343-7326. Fax: (514) 343-2210. E-mail: pascale.legault@umontreal.ca.

[§] University of Georgia.

[||] Université de Montréal.

10.1021/bi0607150 CCC: $33.50
Published on Web 08/10/2006

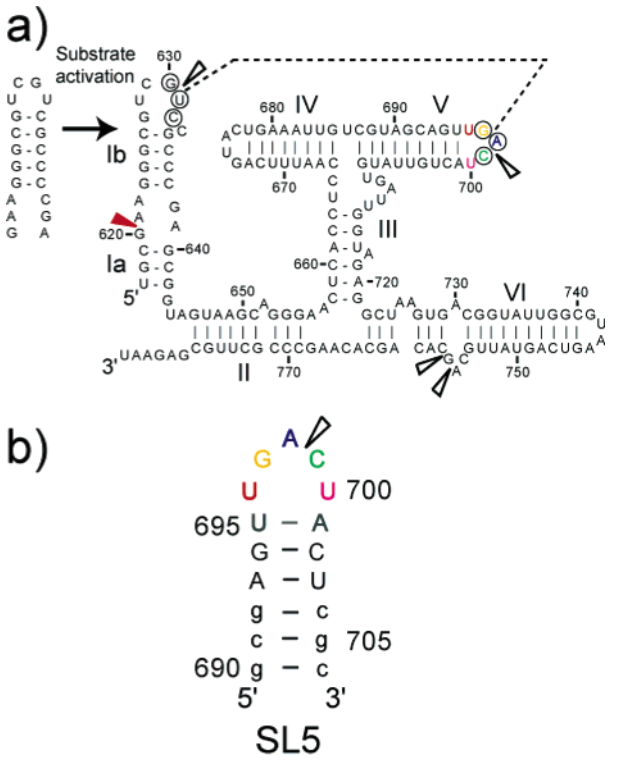

FIGURE 1: Secondary structure and proposed Mg^{2+}-binding sites in the *Neurospora* VS ribozyme. (a) Primary and secondary structures of the VS ribozyme. The cleavage site is designated by the red arrowhead. The interaction between stem−loops I and V is represented as a dashed line, and residues involved in this interaction are circled. Upon interaction with stem−loop V, stem−loop I (subdivided into Ia and Ib) undergoes a structural change from an inactive to an active conformation. (b) Sequence and secondary structure of the stem−loop V RNA (SL5) used for the NMR study. Wild-type and mutant nucleotides are represented as upper- and lowercase letters, respectively. In panels a and b, the empty arrowheads indicate proposed sites of Mg^{2+} binding from phosphorothioate interference and Mn^{2+} rescue experiments (*18*). SL5 nucleotides are color-coded for easy identification in subsequent figures.

and VI to allow the necessary interaction between the cleavage site internal loop and the A730 loop (*10*, *18*). Although models of the tertiary structure have been proposed (*19*, *20*) and NMR structures of individual stem−loop motifs have been determined (*21*−*25*), there is currently no reported high-resolution structure of the VS ribozyme.

Substrate recognition by the VS ribozyme involves tertiary interactions between the substrate and catalytic domains. The best-characterized tertiary interaction is the Mg^{2+}-dependent loop I−loop V interaction, which involves Watson−Crick base pairing between residues 630−632 of stem−loop I and residues 697−699 of stem−loop V (*26*). Formation of this interaction is accompanied by a structural change in stem−loop I, in which nucleotides 623−625 in stem−loop I shift their base paring partners from nucleotides 634−636 to nucleotides 635−637 (Figure 1a), extruding C634 from the stem and rearranging the active site internal loop (Figure 1a) (*14*). Such a conformational change in stem−loop I can be induced by the addition of stem−loop V and Mg^{2+} only (*27*). It has been demonstrated that this conformational change is essential for activation of the stem−loop I RNA (*14*). Indeed, stem−loop I RNA mutants that cannot undergo this conformational change are not cleaved by the VS ribozyme, whereas stem−loop I mutant substrates that can adopt the shifted conformation are active in the cleavage reaction (*14*). NMR structures of both the unshifted (inactive) (*21*, *22*) and shifted (active) (*24*) conformations have been determined by NMR spectroscopy. These structures indicate that the conformational change in stem−loop I leads to the formation of a Mg^{2+}-binding site and of a tertiary interaction motif in the cleavage site internal loop, both of which may be important for catalysis (*24*).

The catalytic activity of the VS ribozyme has a strict requirement for the presence of metal cations with magnesium being the preferred divalent metal ion (*28*, *29*). Other cations such as calcium, manganese, and certain monovalent ions support catalysis, whereas cobalt hexammine [$Co(NH_3)_6^{3+}$][1] supports the correct folding of the ribozyme but not catalysis (*28*−*30*). Phosphorothioate substitution interference and manganese rescue experiments have been used to define sites of divalent cation interaction (Figure 1a) (*18*). Using these methods, Mg^{2+} coordination sites were identified in the A730 loop at the proposed active site (Figure 1a) (*18*). Mg^{2+}-binding sites were also identified in the terminal loops of stem−loops I and V and involve the 5′-phosphates of U631 and C699, two nucleotides that directly participate in the Mg^{2+}-dependent loop I−loop V interaction (Figure 1a). Folding experiments revealed that $Co(NH_3)_6^{3+}$ ions are not as effective at stabilizing either the stem−loop I−stem−loop V interaction or the active (shifted) conformation of stem−loop I, indicating that $Co(NH_3)_6^{3+}$ ions may not fulfill all the roles that Mg^{2+} ions play in this interaction (*30*).

We are using the *Neurospora* VS ribozyme as a model system to investigate various aspects of RNA structure and function. At present, we are pursuing NMR structural studies to gain insight into the substrate recognition and activation by the VS ribozyme (*24*, *25*). We recently determined the three-dimensional structure of stem−loop V in the absence of Mg^{2+}, $SL5^{free}$, by heteronuclear NMR spectroscopy and used chemical shift mapping to understand the effect of Mg^{2+} on the $SL5^{free}$ structure (*25*). As predicted from the loop sequence and site-specific substitution experiments (*26*, *31*), we found that loop residues form a U-turn structure (*25*). U-Turns are architectural motifs found in a large number of RNAs (*32*−*36*) and are often implicated in tertiary interactions (*37*, *38*). In SL5, the consensus UNR sequence (U is uracil, N any base, and R purine) is represented by U696, G697, and A698 (Figure 1). Our NMR structure revealed that the U-turn of $SL5^{free}$ does not meet all the criteria of a canonical U-turn structure (*25*, *32*, *37*, *39*). We also determined that addition of Mg^{2+} resulted in numerous ^1H and ^{13}C chemical shift changes for the SL5 loop (*25*). Given the widespread changes in chemical shifts, it was impossible to precisely locate Mg^{2+}-binding sites from these data.

[1] Abbreviations: SL5, stem−loop 5; $SL5^{free}$, SL5 in the absence of magnesium ions; $SL5^{Mg}$, magnesium ion-bound form of SL5; 1D, one-dimensional; 2D, two-dimensional; 3D, three-dimensional; HSQC, heteronuclear single-quantum coherence; CT-HSQC, constant-time HSQC; COSY, correlated spectroscopy; E. COSY, exclusive COSY; TOCSY, total correlation spectroscopy; HETCOR, heteronuclear correlation; NOE, nuclear Overhauser effect; NOESY, NOE spectroscopy; CPMG, Carr−Purcell−Meiboom−Gill method; HMQC, heteronuclear multiple-quantum correlation; RCSB, Research Collaboratory for Structural Bioinformatics; PDB, Protein Data Bank; rmsd, root-mean-square deviation; $Mn(H_2O)_6^{2+}$, hexahydrated manganese ion(s); $Co(NH_3)_6^{3+}$, cobalt hexammine ion(s).

Furthermore, it was postulated that Mg^{2+} induces a conformational change in the SL5 loop (*25*). In this report, we have determined the NMR structure of SL5 in the presence of Mg^{2+}, $SL5^{Mg}$, and used NMR methods to localize cation-binding sites in $SL5^{Mg}$. Our results improve our understanding of the effect of Mg^{2+} on the stem−loop V U-turn structure and on the formation of the stem−loop I−stem−loop V interaction.

EXPERIMENTAL PROCEDURES

Sample Preparation. Unlabeled, ^{15}N-labeled, and ^{13}C- and ^{15}N-labeled SL5 RNAs (Figure 1b) were synthesized and purified as previously described (*25*). The final concentration of the NMR samples ranged from 0.8 to 2.0 mM SL5 RNA. The sample buffer was exchanged by using Centricon-3 ultrafiltration devices with either NMR buffer A [10 mM d_{11}-Tris (pH 7.0), 50 mM NaCl, and 0.05 mM NaN_3] or NMR buffer B [10 mM d_{11}-Tris (pH 7.0) and 0.05 mM NaN_3], which contained 90% H_2O and 10% D_2O. For studies in D_2O, the RNA samples were transferred to 99.996% D_2O with multiple cycles of lyophilization and resuspension in D_2O. Before addition of metal ions, the RNA samples were heated to 95 °C for 2 min and then immediately cooled in ice and water. The Mg^{2+}-bound form of SL5, $SL5^{Mg}$, was prepared by the addition of 99.995% $MgCl_2$ (Sigma-Aldrich, St. Louis, MO) to the NMR samples; 40 mM $MgCl_2$ was added to RNA samples in NMR buffer A, and either 20 or 46 mM $MgCl_2$ was added to RNA samples in NMR buffer B. We found that these buffer conditions including $MgCl_2$ were essentially equivalent (Figure S1 of the Supporting Information), causing >90% of the total Mg^{2+}-induced chemical shift changes in the loop resonances of SL5.

NMR Spectroscopy. All NMR experiments were conducted at 25 °C on a Varian ^{Unity}INOVA 600 MHz spectrometer equipped with a pulsed field gradient unit and an actively shielded *z* gradient probe, either a $^1H\{^{13}C/^{15}N\}$ triple-resonance probe or a $^1H\{^{15}N-^{31}P\}$ indirect detection probe. Assignment of ^1H, ^{13}C, ^{15}N, and ^{31}P nuclei in $SL5^{Mg}$ was achieved initially by comparing assigned 2D $^1H-^{13}C$ CT-HSQC and $^1H-^{15}N$ HSQC spectra of $SL5^{free}$ with those obtained at the various points of the $MgCl_2$ titrations. The assignment was subsequently completed with 2D and 3D heteronuclear NMR experiments, as described below. All nonexchangeable protons and their attached carbons were assigned from the following experiments collected in D_2O: 2D $^1H-^{13}C$ CT-HSQC (*40*, *41*), 3D HCCH-COSY (*42*), 3D HCCH-TOCSY (*42*), and 3D ^{13}C-edited HMQC-NOESY spectra with mixing times of 75 and 150 ms (*43*). The exchangeable protons and their attached nitrogens were assigned in H_2O from imino- and amino-optimized 2D $^1H-^{15}N$ HSQC (*44*) and 2D $^1H-^{15}N$ CPMG-NOESY (*45*) spectra. A long-range $^1H-^{15}N$ HSQC spectrum collected in D_2O was used for assignment of N1 and N3 of adenines and N7 and N9 of purines ($J = 21$ Hz) (*46*). A 2D $^1H-^{31}P$ HETCOR spectrum collected in D_2O was used for the assignment of the ^{31}P resonances (*47*). Distance restraints were obtained from a 2D $^1H-^{15}N$ CPMG-NOESY (*45*) spectrum collected in H_2O with a mixing time of 150 ms and 3D ^{13}C-edited HMQC-NOESY (*43*) spectra collected in D_2O with mixing times of 75 and 150 ms. The hydrogen bond restraints were determined from $^2J_{NN}$ couplings (*48*, *49*). The standard HNN-COSY spectrum was used to detect $^2J_{NN}$ couplings via the exchangeable imino protons (*48*). Since U695 NH was not detected, we used a modified HNN-COSY experiment to detect the two-bond U695 N3−A701 N1 *J* coupling in the A701·U695 base pair via the nonexchangeable H2 of adenine (*49*). Restraints for the δ torsion angle were obtained from a 3D HCCH E.COSY (*50*) spectrum recorded at 25 °C in D_2O. All NMR spectra were processed with the NMRPipe/NMRDraw package (*51*) and analyzed with NMRView (*52*). ^1H, ^{13}C, and ^{15}N chemical shifts were referenced to an external standard of 2,2-dimethyl-2-silapentane-5-sulfonic acid (DSS) at 0.00 ppm (*53*), and ^{31}P chemical shifts were referenced to an external standard of 85% phosphoric acid at 0.00 ppm.

Structure Calculation. The distance restraints from the 3D ^{13}C-edited HMQC-NOESY spectra were separated into four ranges: strong (1.8−3.0 Å), medium (1.8−4.1 Å), and weak (1.8−5.5 Å) based on the intensities of peaks observed at a mixing time of 75 ms and very weak (1.8−7.0 Å) for signals observed at only the 150 ms mixing time. The distance restraints obtained from the 2D $^1H-^{15}N$ CPMG-NOESY spectra were given ranges of either 1.8−5.5 or 1.8−7.0 Å on the basis of cross-peak intensities. Because of the strong NMR evidence (from NOESY and HNN-COSY spectra) for the formation of the A·U and G·C Watson−Crick base pairs in the stem of $SL5^{Mg}$, canonical distance restraints were employed to define the hydrogen bonding pattern and planarity for the first five base pairs in the stem of $SL5^{Mg}$ (residues 690−694 and 702−706). We obtained limited NOE data for the U695·A701 base pair; therefore, in this case, only the U695 N3−A701 N1 distance was restrained (2.82 ± 0.1 Å) on the basis of the HNN-COSY data. All the sugar puckers except for those of residues 696−700 were set to C3′-endo ($\delta = 86 \pm 10°$) on the basis of 3D HCCH E.COSY data. For residues U696−U700, the $^3J_{H1'-H2'}$ values derived from the HCCH E.COSY data represent the average values of C3′-endo and C2′-endo conformers, indicating that these riboses are in equilibrium between these two conformations. The γ torsion angle restraints were derived from comparative analyses of NOE data (*54*). The γ angles for all the residues, except loop residues 696−700, were set to the gauche$^+$ conformation ($\gamma = 60 \pm 20°$).

Three-dimensional structures were calculated with restrained molecular dynamics and simulated annealing in X-PLOR-NIH version 2.0.6 (*55*, *56*) as described previously (*25*). Starting from a set of 75 structures with randomized torsion angles, we found 69 structures that satisfied the experimental restraints (no distance violation of >0.1 Å and no torsion angle violation of >5°). From these 69 structures, the 10 lowest-energy structures were selected for analysis. These 10 structures were also used to calculate an average structure that was minimized against experimental restraints. All structures were visualized and analyzed with MOLMOL (*57*).

UV Spectroscopy and Determination of T_m Values. Thermal stability studies of SL5 were conducted on purified RNAs with a Cary model 300 UV−visible spectrophotometer equipped with a Peltier heating accessory. All samples contained 10 μM SL5 in NMR buffer B and the indicated metal ions (Figure S3 of the Supporting Information), whereas the RNA was omitted in the control samples (blank). Samples were heated from 10 to 98 °C at a rate of 1 °C/

min, while absorbance data were collected at 260 nm in 1 °C increments. Eighty scans were collected and averaged for each data point in a dual-beam mode with automatic subtraction of the control samples from the RNA samples. Melting temperatures were determined from the second derivative of the absorbance versus temperature curve and linear regression of points on either side of the null for accurate determination of the null. Reported melting temperatures are averaged values derived from two individual UV denaturation profiles.

Metal Ion Binding Studies. A 1.0 mM sample of ^{13}C- and ^{15}N-labeled SL5 in NMR buffer B and 100% D_2O was titrated with $MgCl_2$. The titration was carried out by directly adding increasing amounts of concentrated 99.995% $MgCl_2$ (Sigma-Aldrich) to the RNA sample. The Mg^{2+} concentrations were 0, 0.25, 0.50, 0.75, 1.0, 2.0, 3.0, 5.0, 7.5, 15, 36, and 46 mM. Chemical shift changes were monitored at each $MgCl_2$ concentration by collecting 2D ^{1}H−^{13}C CT-HSQC spectra (*40*, *41*).

A 1.0 mM sample of ^{13}C- and ^{15}N-labeled SL5 in NMR buffer A and 100% D_2O was titrated with $Co(NH_3)_6Cl_3$. The titration was carried out by directly adding increasing amounts of concentrated $Co(NH_3)_6Cl_3$ (Sigma-Aldrich) to the RNA sample. The cobalt hexammine ion concentrations were 0, 0.25, 0.50, 0.75, 1.0, 2.0, 5.0, and 6.0 mM. Chemical shift changes were monitored at each $Co(NH_3)_6Cl_3$ concentration by collecting 2D ^{1}H−^{13}C CT-HSQC spectra (*40*, *41*). NOEs between $Co(NH_3)_6^{3+}$ and SL5 were obtained by collecting 3D ^{13}C- and ^{15}N-edited NOESY-HSQC spectra (*58*) with mixing times of 90 and 180 ms on a 1.0 mM sample of SL5 in NMR buffer A in 90% H_2O and 10% D_2O supplemented with 4 mM $Co(NH_3)_6Cl_3$.

Four $MnCl_2$ titrations were carried out by directly adding increasing amounts of concentrated 99.99% $MnCl_2$ (Sigma-Aldrich) to various RNA samples. The Mn^{2+} concentrations for these titrations were 0, 10, 20, 40, and 80 μM, and the paramagnetic effect of Mn^{2+} was monitored at each of these $MnCl_2$ concentrations. For the first titration, we used a 1.0 mM sample of ^{13}C- and ^{15}N-labeled SL5 in NMR buffer B with 46 mM $MgCl_2$ and 100% D_2O, and the paramagnetic effect was monitored by collecting 2D ^{1}H−^{13}C CT-HSQC spectra (*40*, *41*). A second $MnCl_2$ titration was carried out with a 1.0 mM sample of ^{15}N-labeled SL5 in NMR buffer B with 20 mM $MgCl_2$ and a 90% H_2O/10% D_2O mixture, and the paramagnetic effect was detected by 1D ^{1}H and imino- and amino-optimized 2D ^{1}H−^{15}N HSQC spectra (*44*). A third $MnCl_2$ titration was carried out with a 2.0 mM sample of ^{15}N-labeled SL5 in NMR buffer B with 20 mM $MgCl_2$ and 100% D_2O, and the paramagnetic effect was studied by long-range 2D ^{1}H−^{15}N HSQC spectra optimized for detection of N1 and N3 of adenines and N7 and N9 of purines ($J = 21$ Hz) (*46*). A fourth titration was carried out with a 1.4 mM sample of unlabeled SL5 in NMR buffer B with 46 mM $MgCl_2$ and 100% D_2O, and the paramagnetic effect was detected with 1D ^{31}P spectra (*47*).

Structure Modeling of $Mn(H_2O)_6^{2+}$-Binding Sites. Structures of a complex between $SL5^{Mg}$ and $Mn(H_2O)_6^{2+}$ were obtained by repeating the structure calculation of $SL5^{Mg}$ in the presence of $Mn(H_2O)_6^{2+}$. NMR signals that were broadened to baseline at 20 μM $MnCl_2$ indicated that the nuclei or the pairs of nuclei giving rise to these signals were close in space to $Mn(H_2O)_6^{2+}$. Broadened peaks were found in the 1D ^{31}P, 2D ^{1}H−^{13}C CT-HSQC (*40*, *41*), and 2D ^{1}H−^{15}N HSQC spectra (*44*, *46*), and the nuclei involved are ^{31}P, directly bonded ^{1}H−^{13}C pairs, directly bonded imino and amino ^{1}H−^{15}N pairs, and H2−N3, H2−N1, H8−N7, and H8−N9 pairs. We therefore defined distance restraints between the Mn^{2+} and the nuclei or pairs of nuclei that had their peaks broadened to baseline. For all these distance restraints, we used bounds of 1.8−7.0 Å between the nuclei involved and the Mn^{2+} center of the $Mn(H_2O)_6^{2+}$ complex. Only distance restraints defining $Mn(H_2O)_6^{2+}$-binding sites in the loop (residues U695−A702), but not the stem, were modeled. Four $Mn(H_2O)_6^{2+}$-binding sites were defined (see below). To help localize these $Mn(H_2O)_6^{2+}$ ions, repulsive restraints (>7.0 Å) were used between the four Mn^{2+} centers and nuclei with resonance that exhibited little or no specific line broadening at 80 μM $MnCl_2$. For the structure calculation, we used the same protocol used for NMR structure determination of $SL5^{free}$ (*25*) and $SL5^{Mg}$. However, after randomization of the backbone angles and before the first cycle of high-temperature dynamics, four $Mn(H_2O)_6^{2+}$ were placed linearly at the 3′-end of the SL5 RNA. The coordinates for the $Mn(H_2O)_6^{2+}$ complex were obtained by substituting the magnesium atom in the $Mg(H_2O)_6^{2+}$ complex with a manganese atom. The $Mg(H_2O)_6^{2+}$ coordinates and parameters and the manganese parameters were all obtained from HIC-Up (*59*).

On the basis of the following clustering analysis of nuclei that had their resonance broadened to baseline at 20 μM $MnCl_2$ (Table S3 of the Supporting Information), we inferred four $Mn(H_2O)_6^{2+}$-binding sites in the loop (sites 1−4). The N7 and N9 atoms of G697 and A698 and the H8 and C8 atoms of G697 are on the minor groove side of the loop, whereas the other affected atoms are located on the major groove side. These atoms constitute one Mn^{2+}-binding site. The amino group of C702 is located close to N7 of A701, and this cluster of atoms likely constitutes one binding site. The affected atoms of U696 and the 5′-phosphate of C699 are located too far from each other and therefore likely define two other separate Mn^{2+}-binding sites. In the first round of structure calculation, site 1 was restrained to H6 and C6 of U696. Site 2 was restrained to C8, H8, N7, and N9 of G697 and N7 and N9 of A698. Site 3 was restrained to 5′-phosphate of C699, and site 4 was restrained to N4, H41, and H42 of C702. The other affected atoms (H5 and C5 of U695, H5 and C5 of U696, 5′-P of G697, 5′-P of A698, and N7 and N9 of A701) were restrained to any of the four Mn^{2+} ions. Using four $Mn(H_2O)_6^{2+}$ ions for structure calculation, we easily obtained structures that satisfied all experimental restraints. However, structural calculations using two or three $Mn(H_2O)_6^{2+}$ ions instead of four were unsuccessful, since structures which satisfied all experimentally derived restraints could not be obtained. After an initial round of structure calculation, it was found that H5 and C5 of U695 had a preference for Mn^{2+} at site 3, whereas 5′-P of G697 and 5′-P of A698 had a preference for Mn^{2+} at site 1 and N7 and N9 of A701 a preference for Mn^{2+} at site 4. These atoms were restrained to their preferred $Mn(H_2O)_6^{2+}$ sites for the final round of structure calculation.

In the final round of calculation, 47 of the 50 calculated structures satisfied the experimental restraints (no distance violation of >0.1 Å and no torsion angle violation of >5°). From these 47 structures, the 10 lowest-energy structures

were selected for analysis and were used to calculate an average structure that was minimized against experimental restraints. All structures were visualized and analyzed with MOLMOL (*57*).

RESULTS

$SL5^{Mg}$ Structure Determination. To investigate the solution structure of $SL5^{Mg}$, we used the same 17-nucleotide RNA fragment of stem−loop V, termed SL5, which we previously used for NMR structure determination of $SL5^{free}$ (Figure 1b) (*25*). Although a few base pairs of the stems were mutated to increase synthesis yields (Figure 1b) (*60*), it was previously found that mutations in stem V that do not disrupt base pairing are compatible with catalytic activity (*61*). In addition, chemical modification experiments indicate that SL5 (Figure 1b) supports formation of the active conformation of stem−loop I in the presence of Mg^{2+} (A. Andersen, R. Collins, and P. Legault, unpublished results) (*27*). We have also previously determined that both $SL5^{free}$ and $SL5^{Mg}$ form hairpins under our NMR conditions (*25*), in agreement with the secondary structure model of the VS ribozyme (Figure 1a) (*27*).

The NMR structure of $SL5^{Mg}$ was obtained from standard homonuclear and heteronuclear NMR methods applied to unlabeled, ^{15}N-labeled, and ^{13}C- and ^{15}N-labeled RNAs. Resonance assignment of $SL5^{Mg}$ was substantially facilitated because the complete resonance assignment of $SL5^{free}$ was available (*25*). By carefully tracking peaks in 2D $^{1}H-^{13}C$ CT-HSQC and 2D $^{1}H-^{15}N$ HSQC spectra during the Mg^{2+} titration (*25*), we could obtain the assignment of many ^{1}H, ^{13}C, and ^{15}N resonances for $SL5^{Mg}$. Additional heteronuclear NMR experiments were used to confirm and complete the assignment, as described in Experimental Procedures. A list of the resonance assignments for ^{1}H, ^{13}C, ^{15}N, and ^{31}P nuclei in $SL5^{Mg}$ is provided in Table S1 (Supporting Information).

U-Turn Spectral Characteristics in $SL5^{Mg}$. As was found for $SL5^{free}$, the residues in the stem (690−695 and 701−706) of $SL5^{Mg}$ exhibited spectral characteristics typical of A-form helices (*25*). However, differences in the loop NOEs between $SL5^{free}$ and $SL5^{Mg}$ clearly indicated that Mg^{2+} ions stabilize a more compact SL5 loop structure (data not shown). In both structures, the NOEs from the ribose protons of U696 to G697 H8, A698 H8, and C699 H5 are characteristic of the sharp turn in the loop after U696. However, there is an increase in the NOE intensities between U696 and residues A698 and C699 of $SL5^{Mg}$ in comparison to those of $SL5^{free}$, indicating that U696 is closer to A698 and C699 in $SL5^{Mg}$. For $SL5^{Mg}$, we also noted an increase in the intensity of the NOEs between the ribose of C699 and the base of A701 and the appearance of a NOE between C699 H5 and A701 H2. There was no evidence of stacking between the bases of residues C699 and A701 in $SL5^{free}$; however, these NOE data indicated base stacking between these two residues in $SL5^{Mg}$.

We compared NMR data for $SL5^{Mg}$ with known NMR spectral properties of U-turn structures containing the characteristic U 2′-OH···R N7 and U H3···R 3′-phosphate hydrogen bonds (*62*−*65*). Previously characterized NMR spectral properties of the U-turn are detectable U 2′-OH (∼8.6 ppm) (*65*) and U H3 (∼11−11.5 ppm) protons (*62*, *64*, *65*), a downfield-shifted R N7 (*65*), and downfield-shifted ^{31}P resonances for the UpN and NpR phosphates (*63*−*65*). For $SL5^{Mg}$, the exchangeable U696 2′-OH and H3 protons were not observed at 25 °C. However, in a 1D ^{1}H spectrum collected at 15 °C, we observed low-intensity resonances at 8.8 and 10.6 ppm (not shown), which can be tentatively assigned to the U696 2′-OH and H3 protons, respectively. In 2D NOESY spectra collected at 15 °C, NOEs to other SL5 protons were not observed (not shown), but ^{15}N and ^{13}C decoupling during acquisition indicates that the signal at 8.8 ppm is not directly attached to either a carbon or a nitrogen and that the signal at 10.6 ppm is directly attached to a nitrogen (not shown).

Better evidence of U-turn formation is provided by chemical shift analysis of nonexchangeable resonances. N7 of A698 is the most downfield-shifted N7 resonance (223.1 ppm; Table S1 of the Supporting Information), 7 ppm downfield from its $SL5^{free}$ value (230.1 ppm) (*25*). This downfield shift of A698 N7 is a strong indicator of its participation in a hydrogen bond with U 2′-OH (*65*). In U-turn structures, the α torsion angle of the turning phosphate (UpN) adopts a trans configuration and is involved in binding Mg^{2+}. These two factors are responsible for its downfield-shifted resonance (*63*, *64*). For $SL5^{Mg}$, the phosphorus resonance of the turning phosphate (U696pG697) is the most downfield-shifted ^{31}P resonance (2.18 ppm; Figure S2 and Table S1 of the Supporting Information), 1.8 ppm downfield from its $SL5^{free}$ value (0.37 ppm) (*25*). In a previous NMR study, a downfield-shifted resonance has also been associated with the U-turn NpR phosphate (*65*). For $SL5^{Mg}$, the G697pA698 phosphate yields the second most downfield-shifted ^{31}P resonance (1.12 ppm; Figure S2 and Table S1 of the Supporting Information), 1.1 ppm downfield from its $SL5^{free}$ value (0.05 ppm) (*25*). We also unambiguously assigned the ^{31}P resonance of the A698 3′-phosphate (−1.20 ppm) and found that it is upfield-shifted by 0.8 ppm when compared to its $SL5^{free}$ value (−0.39 ppm) (*25*). This upfield shift may be an indicator of the participation of the A698pC699 phosphate in a hydrogen bond with U696 H3. Indeed, the U H3···R 3′-phosphate hydrogen bond of U-turns is homologous to the G NH2···R 3′-phosphate hydrogen bond of GNRA tetraloops (*66*), and we find a striking similarity of ^{31}P assignment between the U-turn of $SL5^{Mg}$ and GNRA tetraloops. Here, we obtained nonstandard ^{31}P chemical shift values of 2.18, 1.12, and −1.20 ppm for the U, N, and R 3′-phosphates (Figure S2 and Table S1 of the Supporting Information), respectively, whereas ^{31}P chemical shift values of 2.05, 0.67, and −1.07 ppm have been found previously for the G, N, and R 3′-phosphates, respectively, of a small GNRA tetraloop (*67*). In summary, these chemical shift data strongly indicate that Mg^{2+} ions allow the formation of a more compact U-turn structure for SL5, including formation of the two characteristic hydrogen bonds of canonical U-turn structures.

$SL5^{Mg}$ Forms a Canonical U-Turn Structure. To precisely define the structural differences between $SL5^{free}$ and $SL5^{Mg}$, the three-dimensional structure of $SL5^{Mg}$ was determined by NMR, as previously described for $SL5^{free}$ (*25*). The structural statistics (Table 1) of the ensemble of the 10 lowest-energy structures indicate that the structure of $SL5^{Mg}$ is defined well by the NMR data.

As we have found for $SL5^{free}$, $SL5^{Mg}$ forms a hairpin with an A-form stem and a five-membered loop, which adopts a

Table 1: Statistics from the Structure Calculation of $SL5^{Mg}$

no. of distance restraints	408
no. of NOE-derived distance restraints	379
no. from standard NOESY spectra	340
internucleotide	124
intranucleotide	216
no. from 2D $^{1}H-^{15}N$ CMPG-NOESY spectra	39
no. of hydrogen bond restraints	29
no. of dihedral angle restraints	24
sugar pucker (δ)	12
backbone (γ)	12
total no. of restraints	432
rmsd from experimental restraints	
NOE (Å) (none >0.1 Å)	0.005 ± 0.001
dihedral (deg) (none >5°)	0.046 ± 0.011
rmsd from idealized geometry	
bonds (Å)	0.003959 ± 0.000017
angles (deg)	0.960090 ± 0.000573
impropers (deg)	0.362660 ± 0.001690
heavy atom rmsds from the minimized average structure (Å)	
overall (residues 691−705)	1.00 ± 0.23
stem (residues 691−695 and 701−705)	0.51 ± 0.20
loop (residues 696−700)	0.72 ± 0.18

U-turn motif (Figure 2). $SL5^{free}$ and $SL5^{Mg}$ share many of the structural characteristics found in canonical U-turn structures (Figure 2 and Table 2) (*32*, *37*, *39*). In both RNAs, U696, G697, and A698 form the consensus UNR sequence (U is uracil, N any base, and R purine) of U-turn motifs. They both display the sharp turn after U696 that allows backbone reversal and stacking of the G697, A698, and C699 bases after the turn. In $SL5^{free}$, the α torsion angle at the turning phosphate (G697 5′-P) is in an eclipsed conformation with values of $116 \pm 7°$ for the 10 lowest-energy structures (Table 2). However, in $SL5^{Mg}$, this angle is in the staggered trans conformation with values of $167 \pm 34°$ for the 10 lowest-energy structures (Table 2). The short distance between U696 O2′ and A698 N7 in $SL5^{free}$ and $SL5^{Mg}$ indicates that they both form one of the two characteristic hydrogen bonds found in canonical U-turn structures. However, in $SL5^{Mg}$, the U696 O2′−A698 N7 distance is on average 0.7 Å shorter than in $SL5^{free}$ (Table 2). $SL5^{free}$ and $SL5^{Mg}$ share one characteristic that is not observed in canonical U-turns; their flanking base pair is the Watson−Crick U695·A701 base pair, whereas canonical U-turns contain noncanonical flanking base pairs. There are also significant structural differences between the loops of $SL5^{free}$ and $SL5^{Mg}$. In $SL5^{free}$, there is no stacking between the U696 base and the 5′-phosphate of A698. However, this stacking interaction found in canonical U-turns is present in $SL5^{Mg}$. In $SL5^{free}$, there is no evidence for hydrogen bonding between the U696 H3 and 3′-phosphate group of A698. However, the U696 N3−A698 3′-P distance in the 10 lowest-energy structures of $SL5^{Mg}$ is compatible with this hydrogen bond (Table 2), which is characteristic of canonical U-turn structures. In summary, if we exclude the flanking base pair, all the structural characteristics of the canonical U-turn structures are present in $SL5^{Mg}$, whereas many are missing in $SL5^{free}$. As a result, the U-turn backbone fold of $SL5^{Mg}$ is more compact than that previously observed for $SL5^{free}$ (Figure 3).

A superposition of the heavy atoms in the loops (residues U695−A701) of $SL5^{free}$ and $SL5^{Mg}$ illustrates the subtle but important conformational change that results from Mg^{2+} binding (Figure 3). The heavy atom rmsd for this superposition is 2.77 Å, which is significantly larger than the loop heavy atom rmsds reported for the 10 lowest-energy structures of both $SL5^{free}$ [0.53 ± 0.05 Å (*25*)] and $SL5^{Mg}$ [0.72 ± 0.18 Å (Table 1)]. The conformational change that occurs between $SL5^{free}$ and $SL5^{Mg}$ involves primarily the formation of a stacking interaction between the bases of C699 and A701. In $SL5^{Mg}$, the base stacking of C699 with A701 brings C699 closer to U696 by an average distance of 1.6 Å. Two cross-strand hydrogen bonds between U696 and C699 that were not observed in $SL5^{free}$ are now found in $SL5^{Mg}$. They are located (1) between U696 H3 and C699 5′-phosphate, which is characteristic of canonical U-turns (Table 2), and (2) between U696 O2 and C699 NH_2 (distance of 3.36 Å in the average structure). Another significant difference between $SL5^{free}$ and $SL5^{Mg}$ is in the position of U700 (Figure 3). In both cases, the base of U700 is extruded from the other bases of the loop (*25*). In $SL5^{Mg}$, the U700 ribose is also completely extruded from the loop, whereas in $SL5^{free}$, this ribose was found in the usual register between the riboses of C699 and A701. More importantly, whereas the U700 base is found in the major groove stacked on the 5′-phosphate of C699 in $SL5^{free}$, the ribose and base of U700 are found in the minor groove face of the loop in $SL5^{Mg}$ (Figure 3). Since the position of U700 is less well defined than other loop nucleotides in $SL5^{Mg}$ (Figure 2a), all 69 accepted structures were analyzed to ascertain that the conformational characteristics of U700 are defined well by the NMR data. We observed in all structures that the C699 base is stacked on the A701 base and that the ribose and base of U700 are extruded from other loop nucleotides and accessible from the minor groove side of the loop.

The less well-defined position for U700 (Figure 2a) may be due to U700 dynamics and/or the lack of structural constraints for this residue. We have previously studied the internal motion of individual bases for $SL5^{free}$ by measurement of ^{13}C $T_{1\rho}$ relaxation times, and we performed similar studies with $SL5^{Mg}$. However, we observed a systematic decrease in ^{13}C $T_{1\rho}$ relaxation times of aromatic resonances from 18−35 ms for $SL5^{free}$ (*25*) to 6−11 ms for $SL5^{Mg}$ (not shown). These ^{13}C $T_{1\rho}$ data indicate that exchange phenomena on the micro- to millisecond time scale other than base dynamics are involved in $SL5^{Mg}$, such as chemical exchange processes associated with Mg^{2+} binding. These results preclude a detailed analysis of internal base motion for $SL5^{Mg}$.

Effect of Metal Ions on RNA Stability. Since the NMR structural data reveal a more compact U-turn fold for $SL5^{Mg}$ versus $SL5^{free}$, we attempted to determine if Mg^{2+} ions specifically stabilize the SL5 RNA. UV denaturation profiles conducted under various salt and ionic strength (*I*) conditions reveal that SL5 is specifically stabilized by addition of Mg^{2+}. There is an increase in the melting temperature (T_m) of 9 °C, from 73 to ∼82 °C, when buffer conditions are changed from those used for structure determination of $SL5^{free}$ [NMR buffer B and 50 mM NaCl ($I = 0.05$ M)] to those used for structure determination of $SL5^{Mg}$ [either NMR buffer B and 20 mM $MgCl_2$ ($I = 0.06$ M) or NMR buffer B, 50 mM NaCl, and 40 mM $MgCl_2$ ($I = 0.17$ M)] (Figure S3 of the Supporting Information). It is interesting to note that the two conditions used for structure determination of $SL5^{Mg}$, which produce identical $^{1}H-^{13}C$ HSQC spectra (Figure S1 of the Supporting Information), have very different ionic strengths

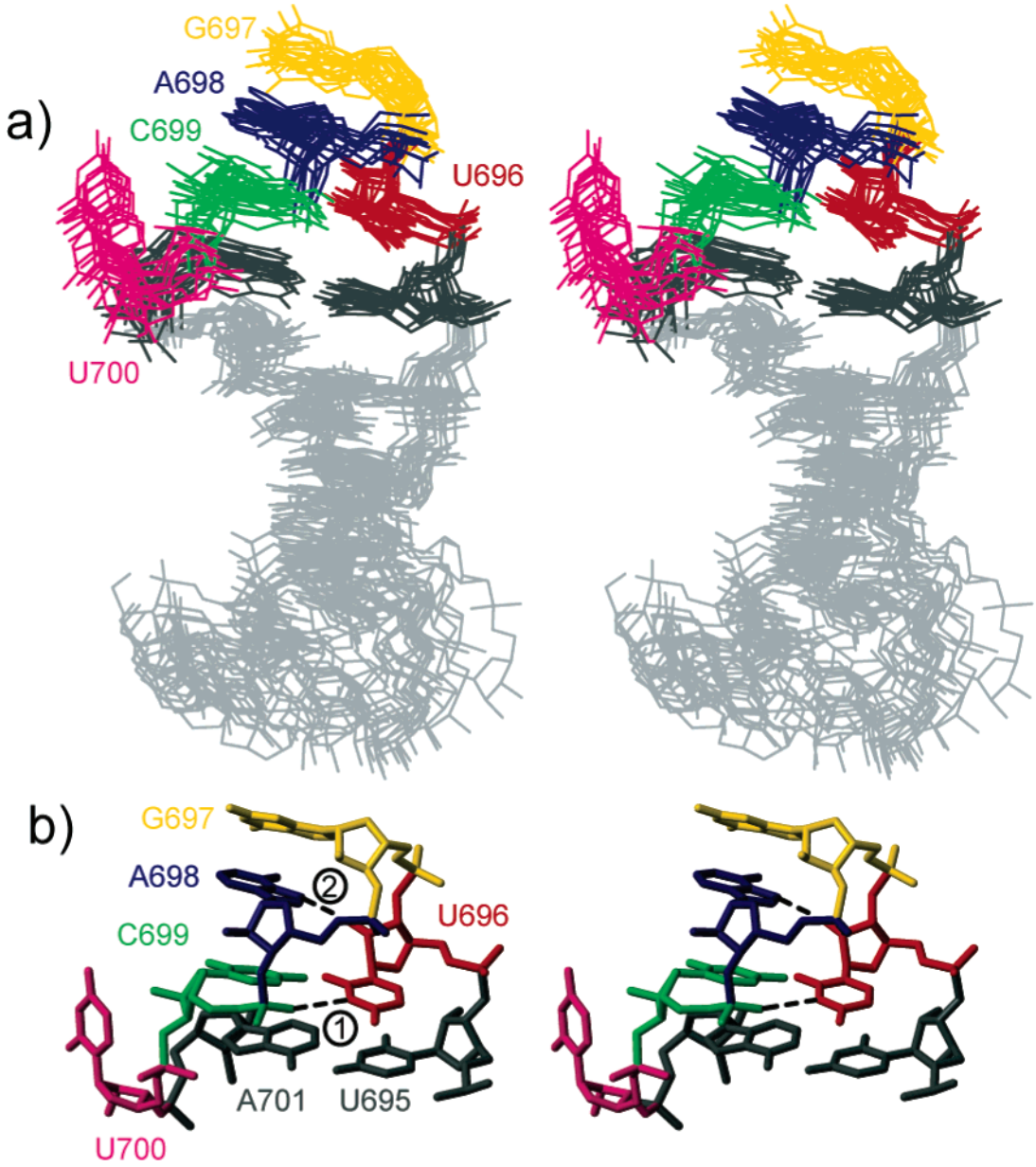

FIGURE 2: Stereoviews of the NMR structure of $SL5^{Mg}$. (a) Superposition of the 10 lowest-energy structures on the minimized average structure. The superposition was obtained by minimization of the pairwise heavy atom rmsd of each lowest-energy structure to the minimized average structure (residues 691−705). (b) Minimized average structure of the loop of $SL5^{Mg}$ showing the two characteristic hydrogen bonds found in U-turn structures: (1) from U696 H3 to A698 3′-phosphate and (2) from U696 2′-OH to A698 N7. For simplicity, only heavy atoms are shown in panels a and b.

but give rise to essentially identical T_m values (82.1 ± 0.5 and 81.5 ± 0.5 °C) (Figure S3 of the Supporting Information). These data indicate that the increase in melting temperature is not simply a result of increased ionic strength (I) and likely results from specific magnesium ion binding. The T_m values for SL5 at a high concentration of a monovalent salt [NMR buffer B and 500 mM NaCl (I = 0.5 M)] further support this conclusion, since under these conditions the T_m remains lower (80.2 ± 0.5 °C) than that obtained with an ~10-fold lower ionic strength when magnesium is the only added salt [NMR buffer B and 20 mM $MgCl_2$ (I = 0.06 M)] (Figure S3 of the Supporting Information). Interestingly, these thermodynamic results correlate well with our NMR chemical shift data demonstrating that the ^1H and ^{13}C chemical shift changes for loop residues are smaller with addition of 500 mM NaCl (*25*) than with addition of 20 mM $MgCl_2$ (Figure S1b of the Supporting Information).

Elucidation of Cation-Binding Sites in $SL5^{Mg}$. Two methods were employed to identify potential Mg^{2+} ligands in $SL5^{Mg}$: NOEs to cobalt hexammine ions [$Co(NH_3)_6^{3+}$] and paramagnetic line broadening caused by Mn^{2+}. Both methods involved direct detection of metal cations that may bind to similar sites and in a manner similar to that of Mg^{2+} (*68*−*70*).

Chemical shift changes upon addition of $Co(NH_3)_6^{3+}$ are very similar to those observed upon addition of Mg^{2+} (Figure S1 of the Supporting Information) (*25*). Although the magnitudes of the chemical shift changes with $Co(NH_3)_6^{3+}$ are slightly different than with Mg^{2+}, the direction of the changes (upfield or downfield) is generally the same in both the ^1H and ^{13}C dimensions. These results indicate that Co-

Table 2: Comparison of the Canonical U-Turn Structural Characteristics of $SL5^{free}$ and $SL5^{Mg}$

U-turn characteristic	$SL5^{free}$	$SL5^{Mg}$
UNR sequence	yes (U696, G697, and A698)	yes (U696, G697, and A698)
noncanonical flanking base pair	no (flanking base pair is the Watson−Crick U695·A701 base pair)	no (flanking base pair is the Watson−Crick U695·A701 base pair)
sharp turn in backbone	yes (G697 α angles are 116 ± 7° in the 10 lowest-energy structures)	yes (G697 α angles are 167 ± 34° in the 10 lowest-energy structures)
stacking of bases immediately after turn	yes (stacking of G697, A698, and C699)	yes (stacking of G697, A698, and C699)
stacking of U base and R 5′-phosphate group	no	yes
hydrogen bond between U 2′-OH and R N7	yes (U696 O2′−A698 N7 distance range in the 10 lowest-energy structures, 2.91−3.93 Å)	yes (U696 O2′−A698 N7 distance range in the 10 lowest-energy structures, 2.45−2.95 Å)
hydrogen bond between U H3 and R 3′-phosphate group	no (U696 N3−A698 3′-P distance range in the 10 lowest-energy structures, 8.19−9.18 Å)	yes (U696 N3−A698 3′-P distance range in the 10 lowest-energy structures, 4.06−5.25 Å)

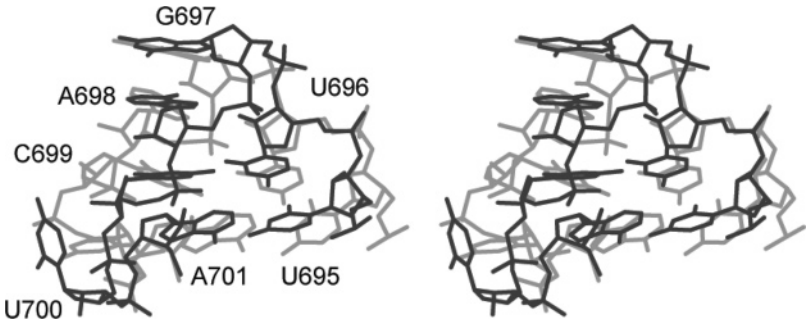

FIGURE 3: Conformational change in the loop of SL5 upon Mg^{2+} binding. The heavy atom superposition of the loop residues (U695−A701) from the minimized average structures of $SL5^{free}$ (light gray) (*25*) and $SL5^{Mg}$ (dark gray) is shown as a stereoview. The heavy atom rmsd for this superposition is 2.77 Å. For simplicity, only heavy atoms are shown.

$(NH_3)_6^{3+}$ likely triggers a conformational change similar to that of Mg^{2+} in the SL5 loop but may not bind to identical sites or in the exact same manner as Mg^{2+} (*71*). Since $Co(NH_3)_6^{3+}$ does not give up its NH_3 ligands, it only exhibits an outer-sphere binding mechanism (*70*). Therefore, the binding of $Co(NH_3)_6^{3+}$ gives an indication of where hexahydrated Mg^{2+} may bind but may not explain all possible Mg^{2+}-binding sites. Mg^{2+} can exhibit several binding modes in aqueous solution, including outer- and inner-sphere mechanisms when binding to RNA (*72*).

NOEs to cobalt hexammine ions were obtained from 3D ^{13}C-edited and ^{15}N-edited NOESY-HSQC spectra (*58*). The 18 protons of $Co(NH_3)_6^{3+}$ resonated at a single frequency of 3.60 ppm, showing that the cobalt hexammine ion is free to rotate in the bound conformation and is in fast exchange between the bound and unbound states (*73*). This means that on the chemical shift time scale, a single cobalt hexammine ion is free to interact with more than one binding site. This behavior has been seen for other RNAs that have been shown to bind $Co(NH_3)_6^{3+}$ by NMR spectroscopy (*73*−*75*). SL5 protons that exhibited a NOE cross-peak to $Co(NH_3)_6^{3+}$ are mapped on the structure of the $SL5^{Mg}$ loop (Figure 4a) and are listed in Table S2 (Supporting Information). NOEs to $Co(NH_3)_6^{3+}$ are observed for protons in the major groove of the stem as well as for U695 H5 and H6 and U696 H5 protons, which are located on the major groove face of the loop (Figure 4a). NOEs to $Co(NH_3)_6^{3+}$ may result from multiple discrete $Co(NH_3)_6^{3+}$-binding sites or diffuse binding along the major groove. Given the complexity of the data, we did not attempt to localize binding sites for $Co(NH_3)_6^{3+}$ in $SL5^{Mg}$.

Mn^{2+} is a paramagnetic ion that specifically broadens the line width of any nuclei that are in its proximity (within ~10 Å) (*76*). This paramagnetic line broadening is a through-space effect and is proportional to r^{-6}, where r is the distance between the Mn^{2+} and the observed nuclei (*76*). Mn^{2+} like Mg^{2+} can exhibit both outer- and inner-sphere binding modes. We used Mn^{2+} to probe for Mg^{2+}-binding sites in $SL5^{Mg}$. The specific samples and experiments employed to detect line broadening of potential metal ligands are listed in Experimental Procedures. An example of the paramagnetic effect of Mn^{2+} on the H6−C6/H8−C8 region of the 2D $^1H-^{13}C$ CT-HSQC spectra of $SL5^{Mg}$ is given in Figure 5. At micromolar Mn^{2+} concentrations, we observed specific line broadening effects (Figure 5). It should be noted that since the titration was carried out in the presence of near-saturating amounts of $MgCl_2$, the addition of Mn^{2+} did not affect chemical shifts. The ^1H, ^{13}C, ^{15}N, and ^{31}P atoms which had their resonances broadened to baseline by addition of 20 μM $MnCl_2$ are listed in Table S3 (Supporting Information), and these results are mapped on the structure of the $SL5^{Mg}$ loop (Figure 4b). Almost every atom that gave a NOE to $Co(NH_3)_6^{3+}$ is affected by Mn^{2+} (Tables S2 and S3 of the Supporting Information). However, Mn^{2+} affected more sites in the loop of $SL5^{Mg}$ than $Co(NH_3)_6^{3+}$ (Figure 4). Indeed, except for U700, all residues in the loop are affected by 20

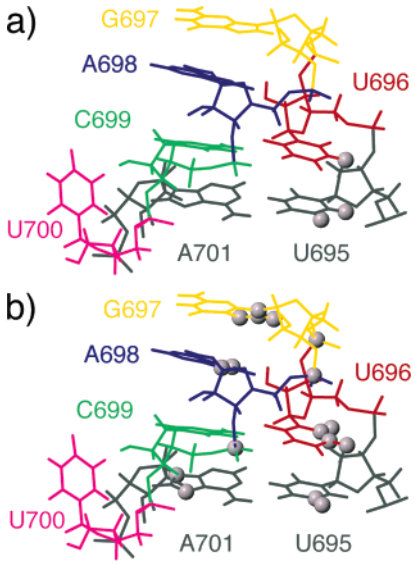

FIGURE 4: Interaction of $Co(NH_3)_6^{3+}$ and Mn^{2+} with the loop of $SL5^{Mg}$. (a) Protons that gave NOEs to $Co(NH_3)_6^{3+}$ were mapped as spheres on the corresponding atoms of the minimized average structure of $SL5^{Mg}$ (U695 H5, U695 H6, and U696 H5). (b) Nuclei that gave rise to resonances broadened below baseline in the presence of 20 μM Mn^{2+} were mapped as spheres on the corresponding atoms of the minimized average structure of $SL5^{Mg}$ (U695 C5 and H5, U696 C5 and H5, U696 C6 and H6, G697 5′-P, G697 C8 and H8, G697 N7 and N9, A698 5′-P, A698 N7 and N9, C699 5′-P, and A701 N7 and N9).

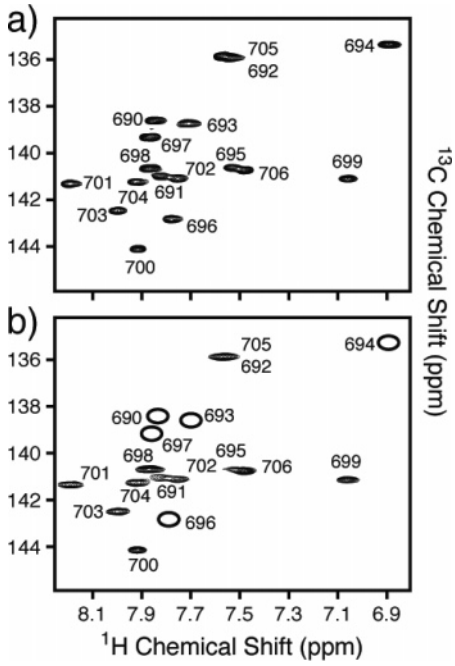

FIGURE 5: Paramagnetic effect of Mn^{2+} on $SL5^{Mg}$. The H6−C6/H8−C8 region of 2D ^{1}H−^{13}C CT-HSQC spectra of $SL5^{Mg}$ in the presence of (a) 0 and (b) 20 μM $MnCl_2$. These spectra were collected in 100% D_2O at 25 °C on a 600 MHz NMR spectrometer. Those peaks that disappear below the baseline level are denoted with empty ovals.

μM Mn^{2+} (Figure 4b). We used these data to localize divalent cation-binding sites.

Structure Modeling of $SL5^{Mg}$ with $Mn(H_2O)_6^{2+}$. To obtain model structures of $Mn(H_2O)_6^{2+}$ bound to the loop of $SL5^{Mg}$, we repeated our structure calculation of $SL5^{Mg}$ after adding distance restraints derived from the paramagnetic effect of Mn^{2+}. To determine the number of bound $Mn(H_2O)_6^{2+}$ ions, we initially circumscribed clusters of atoms close to each other in space among those that were affected by 20 μM $MnCl_2$ (see Experimental Procedures). We defined four Mn^{2+}-binding sites in the loop with this approach. Restraints between the manganese center of the $Mn(H_2O)_6^{2+}$ ions and the $SL5^{Mg}$ loop atoms that were specifically broadened to baseline in the presence of 20 μM $MnCl_2$ (Table S3 of the Supporting Information) were conservatively set to 1.8−7.0 Å. To better position the ions within the binding sites, repulsive restraints (>7.0 Å) were added for those atoms that did not experience any line broadening in the presence of 80 μM $MnCl_2$ (Table S3 of the Supporting Information). An initial round of structure calculation was performed to refine our set of distance restraints to the four $Mn(H_2O)_6^{2+}$ ions (see Experimental Procedures). For the final round of structure calculation, the structural statistics (Table S4 of the Supporting Information) indicate that the structure of $SL5^{Mg}$ with $Mn(H_2O)_6^{2+}$ is defined well by the NMR data, including the loop structure with the four modeled $Mn(H_2O)_6^{2+}$ ions.

The superposition of the loops from the 10 lowest-energy structures on the minimized average structure of $SL5^{Mg}$ modeled with four $Mn(H_2O)_6^{2+}$ ions is shown in Figure 6a. The average heavy atom rmsd for this superposition (residues G694−C702) is 0.63 Å, whereas a similar superposition of the $SL5^{Mg}$ loop structure determined in the absence of Mn^{2+} gave a rmsd of 0.73 Å. A similar superposition of the two minimized average structures (not shown), $SL5^{Mg}$ and $SL5^{Mg}$ with $Mn(H_2O)_6^{2+}$, gives a rmsd of 0.78 Å, indicating that the additional structural constraints for the modeling of the Mn^{2+}-binding sites did not significantly perturb the $SL5^{Mg}$ loop structure. The superposition in Figure 6a also shows that the Mn^{2+} position is slightly better defined at sites 1 and 4 than at sites 2 and 3.

To understand how manganese ions are coordinated in the SL5 loop, we identified potential ligands that were within 4.0 Å of the oxygen atoms of $Mn(H_2O)_6^{2+}$ (Table 3). Three of the Mn^{2+} are directly coordinated to at least one of the residues, U696, G697, and A698, that defined the UNR sequence of the U-turn motif. The Mn^{2+} at site 1 is coordinated to a pocket formed by the 5′-phosphate groups of U696, G697, and A698. The Mn^{2+} at site 2 is coordinated to O2′ of U696 and the N7 atoms of G697 and A698, whereas the Mn^{2+} at site 3 is coordinated to the O4 atoms of U696 and U695, as well as the nonbridging oxygens of the 5′-phosphate of C699. The Mn^{2+} at site 4 is coordinated to the nonbridging oxygens of the 5′-phosphate of U700, O3′ of U700, and N7 of A701 (Table 3). Site 2 is located in the minor groove, whereas sites 1, 3, and 4 are in the major groove. These three Mn^{2+} ions contact at least one oxygen of each of the six 5′-phosphate groups of the SL5 loop (696−701), pointing to the importance of divalent cations in charge neutralization that promote formation of the canonical U-turn fold.

DISCUSSION

Mg^{2+} Stabilizes a Canonical U-Turn Fold for Stem−Loop V of the VS Ribozyme. Substrate recognition by the *Neurospora* VS ribozyme involves the formation of a Mg^{2+}-dependent loop−loop interaction between the stem−loop I substrate and stem−loop V of the catalytic domain. To better understand this important tertiary interaction in the VS

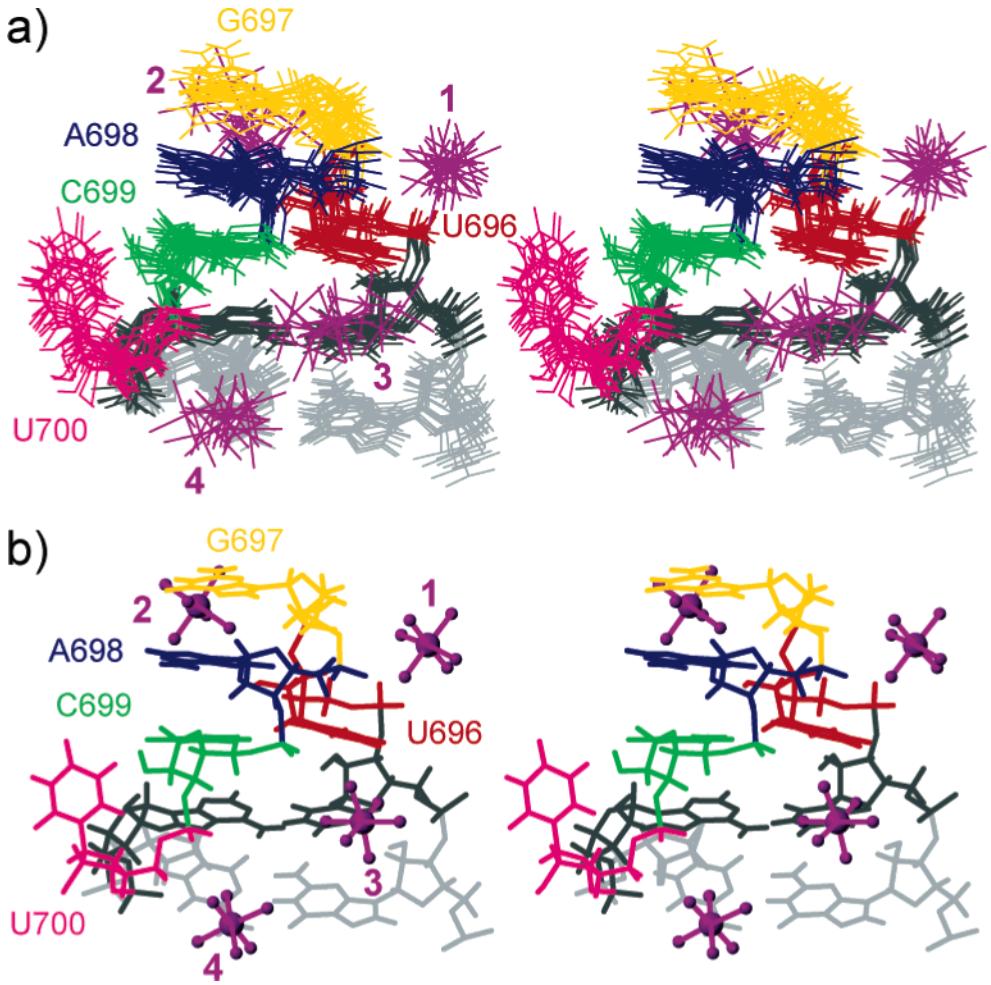

FIGURE 6: Localization of divalent cation-binding sites in $SL5^{Mg}$. (a) Superposition of the 10 lowest-energy structures of $SL5^{Mg}$ modeled with four $Mn(H_2O)_6^{2+}$ complexes. The superposition was obtained by minimizing the rmsd for heavy atoms of residues 694−702. (b) Minimized average structure of $SL5^{Mg}$ modeled with four $Mn(H_2O)_6^{2+}$ complexes. In panels a and b, only residues G694−C702 are shown. The $Mn(H_2O)_6^{2+}$ complexes are numbered from 1 to 4 as described in the text.

Table 3: List of Possible Coordination Sites for $Mn(H_2O)_6^{2+}$ from the Modeling of $Mn(H_2O)_6^{2+}$ to the Loop of $SL5^{Mg}$

$Mn(H_2O)_6^{2+}$ site	coordinating atoms[a]
1	696 5′-O1P, 5′-O2P, O5′
	697 5′-O1P, O3′
	698 5′-O1P, 5′-O2P
2	696 O2′
	697 N7
	698 N7
3	695 O4
	696 O4,
	699 5′-O1P, 5′-O2P
4	700 5′-O1P, O3′
	701 N7

[a] The coordinating atoms were obtained by selecting all hydrogen bond acceptors that were within 4.0 Å of a $Mn(H_2O)_6^{2+}$ oxygen in the minimized average structure.

ribozyme, we have determined the NMR structure of the stem−loop V receptor RNA in the absence [$SL5^{free}$ (*25*)] and presence [$SL5^{Mg}$ (this study)] of Mg^{2+}. Comparison of the NMR data and the calculated structures reveals that Mg^{2+} induces a conformational change in the loop structure of stem−loop V. UV denaturation profiles under various salt conditions confirm that stem−loop V is specifically stabilized by magnesium ions.

In the absence of Mg^{2+}, the terminal loop of SL5 forms a loose U-turn motif with some but not all characteristics of canonical U-turn structures (Table 2) (*25*, *32*, *37*, *39*). The U-turn of $SL5^{free}$ is unusual in that its closing base pair is the Watson−Crick U695·A701 base pair (Table 2). Two other canonical U-turn characteristics are missing for $SL5^{free}$: the stacking of the U696 base on the A698 5′-phosphate and the hydrogen bond between U696 N3 and the A698 3′-phosphate (Table 2). We previously proposed that the longer C1′−C1′ distance of the closing Watson−Crick base pair prevents formation of these canonical U-turn features for SL5 in the absence of Mg^{2+} (*25*). In the presence of Mg^{2+}, the terminal loop of SL5 forms a more compact U-turn structure. Although the closing base pair remains a Watson−Crick U·A base pair, all other canonical U-turn characteristics are present, including the two that were missing from $SL5^{free}$ (Table 2).

In both $SL5^{free}$ and $SL5^{Mg}$, there is a sharp turn after U696 that allows backbone reversal and stacking of the G697, A698, and C699 bases after the turn. However, in $SL5^{Mg}$, the α torsion angle of the turning phosphate adopts a more ideal trans conformation, which brings the 5′-phosphates of U696, G697, and A698 closer to one another, creating a phosphate cluster at the site of backbone reversal (Table 2

and Figure 3). In $SL5^{Mg}$, the base stacking of C699 with A701, which brings C699 closer to U696, also brings the 5′-phosphate groups of G697, A698, C699, and U700 closer to that of U696. The more compact backbone fold of $SL5^{Mg}$ is associated with a more condensed electronegative surface on the major groove face of the SL5 loop.

Cation-Binding Sites in Stem−Loop V of the VS Ribozyme. Mg^{2+}-induced paramagnetic line broadening was detected for specific resonances of SL5, in the presence of a near-saturating amount of Mg^{2+}, and used to model the binding of $Mn(H_2O)_6^{2+}$ to the loop of $SL5^{Mg}$. We found four sites of Mn^{2+} coordination in the loop of $SL5^{Mg}$. The negative charge clustering of the 5′-phosphates of U696, G697, and A698 is stabilized by the presence of one Mn^{2+} (Figure 6, site 1). A second Mn^{2+} interacts with the minor groove face of the loop, and potential ligands are O2′ of U696 and the exposed N7 atoms of G697 and A698 (Figure 6, site 2). A third Mn^{2+} located in the center of the major groove is liganded by the base O4 atoms of U695 and U696 on the 5′-strand and the 5′-phosphate of C699 on the 3′-strand (Figure 6, site 3). The divalent cation at site 3 likely stabilizes the cross-strand hydrogen bond between U696 H3 and the 5′-phosphate of C699, which was absent in $SL5^{free}$. The Mn^{2+} at site 4 involves coordination by the U700 5′-phosphate and N7 of A701. This Mn^{2+} may help to stabilize the extruded ribose conformation at U700. The spatial arrangement of potential ligands at site 2 is similar in $SL5^{free}$ and $SL5^{Mg}$ structures but unique to $SL5^{Mg}$ at sites 1, 3, and 4, indicating that divalent cations at these three sites stabilize the canonical U-turn structure in stem−loop V.

In agreement with our NMR data, coordination of Mn^{2+} to the 5′-phosphate of C699 (Figure 6, site 3) has been previously inferred from manganese rescue of the phosphorothioate interference (Figure 1; *18*). In contrast, the phosphorothioate interference experiment did not identify the phosphate cluster at site 1 or the U700 5′-phosphate at site 4 (*18*). The interference experiment was set up such that on average only one phosphate per RNA was modified; therefore, perturbation at only one of the three phosphate ligands may not have been sufficient to completely inhibit metal ion coordination at site 1. Alternatively, cation binding at sites 1 and 4 may be stabilized by other ligands present in the RNA or from bound water or may not be essential for VS ribozyme function.

Like Mg^{2+}, Mn^{2+} forms a hexahydrated complex in aqueous solution that can exchange one or more water molecules to bind RNA ligand(s) directly (inner-sphere mechanism). We used $Mn(H_2O)_6^{2+}$ for modeling divalent cation-binding sites in $SL5^{Mg}$, although the exact hydration number of the Mn^{2+} was unknown. However, the structural model can be examined in light of our studies with $Co(NH_3)_6^{3+}$, which exhibit only outer-sphere metal ion coordination. In the SL5 loop, NOEs were observed between $Co(NH_3)_6^{3+}$ and U695 H5, U695 H6, and U696 H5, as well as C702 amino protons (Table S2), indicating that $Co(NH_3)_6^{3+}$ may interact with ligands similar to Mg^{2+} at sites 1, 3, and 4 of stem−loop V (Figure 6). These sites may therefore accommodate an outer-sphere mode of metal ion binding. The absence of $Co(NH_3)_6^{3+}$ binding at site 2 suggests that at this site Mg^{2+} binds to some of its RNA ligands via inner-sphere coordination. Differences in ligand-binding sites between Mg^{2+} and $Co(NH_3)_6^{3+}$ were not fully investigated here but may explain, at least partly, why $Co(NH_3)_6^{3+}$ ions are not as effective as Mg^{2+} at stabilizing the interaction between stem−loop I and stem−loop V (*30*).

Similarities with Mg^{2+}-Binding Sites of Other U-Turn Structures. Three of the four Mn^{2+}-binding sites in $SL5^{Mg}$ involve the conserved UNR residues of the U-turn motif (Figure 6, sites 1−3). Similar Mg^{2+}-binding sites have been previously identified in U-turns of other RNA structures (Figure 7). In the crystal structure of the 30S ribosomal unit of *Thermus thermophilus* in complex with a messenger RNA fragment and the anticodon stem−loop motif of $tRNA^{Phe}$ (*77*), there is a canonical U-turn in the anticodon loop fragment of $tRNA^{Phe}$ (Figure 7a). In this RNA, the UNR sequence corresponds to residues U14, G15, and A16, and the loop is closed by a noncanonical U·U base pair between residues U13 and U20 (Figure 7a). There are three Mg^{2+} ions bound to this anticodon loop (Figure 7a), and these three sites are analogous to sites 1−3 in the U-turn of $SL5^{Mg}$ (Figure 6). These sites involve the same RNA ligands identified in $SL5^{Mg}$: the three-phosphate cluster of the UNR residues at site 1, the O2′ atom of U14 and the N7 atoms of G15 and A16 at site 2, and O4 of U14 and the 3′-phosphate of A16 at site 3. In the crystal structure of $tRNA^{Ile}$ complexed with isoleucyl transfer RNA (tRNA) synthetase and mupirocin, there is a canonical U-turn in the unmodified $tRNA^{Ile}$ TψC loop (Figure 7b) (*78*). In this RNA, the UNR sequence corresponds to residues U55, C56, and A57, and the loop is closed by a noncanonical reverse Hoogsteen U·A base pair involving residues U54 and A58 (Figure 7b). There are two $Mg(H_2O)_6^{2+}$ ions bound to this TψC loop (Figure 7b), and these two sites are analogous to sites 1 and 3 in the U-turn of $SL5^{Mg}$ (Figure 6). Since in this U-turn the N residue is a pyrimidine (C56), there is a missing N7 ligand, and this may prevent formation of a site analogous to site 2 in $SL5^{Mg}$. The two cation-binding sites in this loop involve RNA ligands similar to those identified in $SL5^{Mg}$: the three-phosphate cluster of the UNR residues at site 1 and the O4 atoms of U54 and U55 and the 3′-phosphate of A57 at site 3. Mg^{2+} binding at sites equivalent to sites 1 and 3 in $SL5^{Mg}$ occurs in many RNAs and likely plays an important role in stabilizing U-turn motifs.

Implications for Substrate Recognition in the VS Ribozyme. An important step in the catalytic activity of the *Neurospora* VS ribozyme is the formation of a Mg^{2+}-dependent loop−loop interaction between stem−loops I and V. This tertiary interaction is important for recognition and activation of the stem−loop I substrate (*14*). Biochemical studies have shown that an isolated stem−loop V can replace the VS catalytic domain (stem−loops II−VI, Figure 1a) in allowing the tertiary interaction with stem−loop I and in triggering the conformational change in stem−loop I (*27*). Biophysical studies of isolated stem−loops I and V are therefore relevant to understanding the tertiary interaction between stem−loops I and V within the context of the active VS ribozyme. Given that Mg^{2+} ions are required for the loop I−loop V interaction, this NMR study, which thoroughly analyzed the effect of Mg^{2+} on the isolated stem−loop V, allows us to better understand the role of Mg^{2+} in substrate recognition by the VS ribozyme.

The interaction between stem−loop I and stem−loop V involves the formation of Watson−Crick base pairs between stem−loop I residues 630−632 and stem−loop V residues

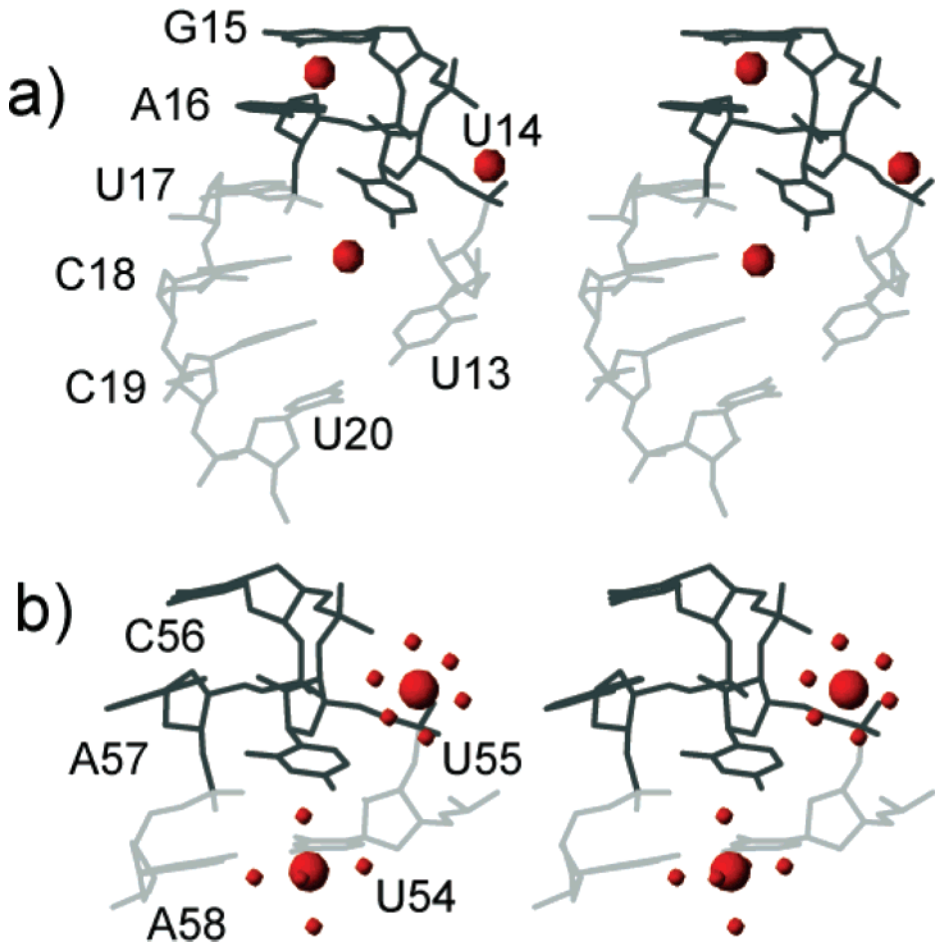

FIGURE 7: Examples of Mg^{2+}-binding sites in U-turns. (a) U-Turn motif found in the anticodon loop of $tRNA^{Phe}$ from the crystal structure of the 30S ribosomal unit in complex with a messenger RNA fragment and the anticodon stem−loop motif of $tRNA^{Phe}$ (PDB entry 1IBL) (*77*). Three Mg^{2+} ions were found associated with this U-turn at sites analogous to sites 1−3 of $SL5^{Mg}$. (b) U-Turn motif found in the $tRNA^{Ile}$ TψC loop from the crystal structure of $tRNA^{Ile}$ in complex with isoleucyl transfer RNA (tRNA) synthetase and mupirocin (PDB entry 1FFY) (*78*). The two $Mg(H_2O)_6^{2+}$ ions are found in sites analogous to sites 1 and 3 of $SL5^{Mg}$.

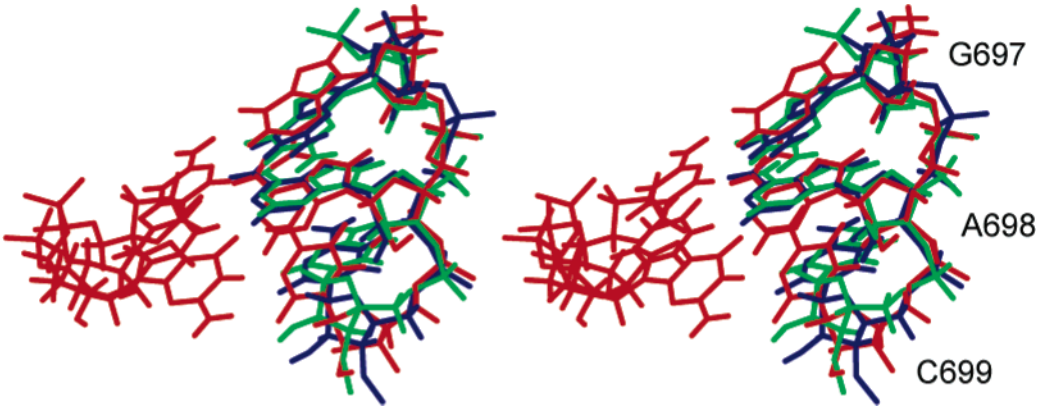

FIGURE 8: Model of base pairing interactions between stem−loop I and stem−loop V. Stereoview of the minimized average structure of $SL5^{free}$ (green) and $SL5^{Mg}$ (blue) superimposed on the structure of a 3 bp A-form helix (red) formed between a 5′-GAC-3′ sequence and a 5′-CUG-3′ sequence. The superposition was obtained by pairwise minimization of the heavy atom rmsd between the bases of the 5′-GAC-3′ sequences (1.66 Å for $SL5^{free}$ and 1.30 Å for $SL5^{Mg}$). Only residues G697, A698, and C699 are shown for $SL5^{free}$ and $SL5^{Mg}$.

G697−C699 (*26*). Although the conformation of the three consecutive loop−loop Watson−Crick base pairs is currently unknown, it likely resembles a short A-form helix. In $SL5^{free}$ and $SL5^{Mg}$, the three bases after the turn (G697, A698, and C699) are stacked on each other with their Watson−Crick faces exposed to the solvent. To verify that this conformation is compatible with A-form base pairing, we previously superposed the heavy atoms of nucleotides G697−C699 in $SL5^{free}$ with those of an equivalent trinucleotide forming an ideal A-form helix (Figure 8) (*25*). Here, we performed the same superposition with $SL5^{Mg}$ and obtained a similar good fit, with the heavy atom rmsd slightly improving from 1.66 Å for $SL5^{free}$ to 1.30 Å for $SL5^{Mg}$ (Figure 8). Although the bases of the proposed Watson−Crick interactions are oriented

slightly more favorably for hydrogen bonding in $SL5^{Mg}$, this likely does not justify by itself the need for Mg^{2+} in stabilizing the loop I−loop V interaction.

We observed that Mg^{2+} ions play an important role in neutralizing electronegative charges in the loop of $SL5^{Mg}$, and this must certainly be important for binding to stem−loop I, which also carries electronegative charges in its loop. In addition, Mg^{2+} ions also bring about important structural changes in the minor groove face of the SL5 loop that may play a role in stem−loop I binding. First, the divalent cation at site 2 could contact stem−loop I ligands in the interaction between stem−loop I and stem−loop V and form a bridge between the two loops. However, mutagenesis of the proposed interloop G697•C632 base pair to a C697•G632 base pair with concomitant removal of one of the N7 ligands at site 2 leads to a 2-fold decrease in the rate of VS self-cleavage (*26*), indicating that divalent cation binding at site 2 does not play a major role in the loop I−loop V interaction. Second, a significant conformational change between $SL5^{free}$ and $SL5^{Mg}$ involves U700, which becomes completely exposed to the solvent on the minor groove face of the loop, in the proximity of the bases of G697−C699. U700 may provide a unique recognition surface for stem−loop I (Figure 3). The importance of this residue in the formation of the tertiary interaction remains to be investigated.

Like stem−loop V, the terminal loop of stem−loop I contains a UNR sequence (U628, C629, and G630). Formation of a U-turn structure in stem−loop I has been postulated from NAIM analysis and site-specific substitutions (*26*, *31*, *79*). A structure of wild-type stem−loop I was determined by NMR spectroscopy in the absence of multivalent metal ions, and it was found that the terminal loop is disordered under those conditions (*21*). Interestingly, phosphorothioate interference and Mn^{2+} rescue experiments suggest divalent metal binding at the 3′-phosphates of G630 in stem−loop I (*18*). In the context of the U-turn motif, this 3′-phosphate is equivalent to the 3′-phosphate of A698 in stem−loop V, which we identified here as a Mg^{2+} ligand (Figure 6, site 3). Mg^{2+} may also support the formation of a U-turn structure in stem−loop I. Hence, some of the roles of magnesium ions in the VS ribozyme may be the stabilization of optimal loop conformations in both stem−loops I and V and the neutralization of electronegative charges in these loops, which would enable formation of an optimal loop I−loop V interaction for catalysis.

CONCLUSION

In the absence of Mg^{2+}, the loop V of the VS ribozyme adopts a loose U-turn fold to accommodate the closing Watson−Crick base pairs and to weaken the repulsion between phosphate groups. Binding of Mg^{2+} in the loop counteracts the negative electrostatic forces created by nearby phosphate groups, helps overcome the constraint placed on the loop by the closing Watson−Crick base pair, and allows formation of a canonical U-turn fold in stem−loop V. In both $SL5^{free}$ and $SL5^{Mg}$, the three residues after the turn (G697, A698, and C699) adopt an A-form structure that exposes their Watson−Crick faces and that is compatible with base pairing to stem−loop I. However, with the changes in the conformation of U700, $SL5^{Mg}$ presents a different recognition surface in the minor groove that may allow additional contacts with stem−loop I. Structural studies of the interaction between stem−loop I and stem−loop V are necessary to further understand the molecular details of substrate recognition by the VS ribozyme and to build on our understanding of the role that Mg^{2+} ions play in this RNA recognition event.

ACKNOWLEDGMENT

We thank members of the Legault laboratory, P. Lampron for wet lab management, R. Richter for computer system management and for providing a script for analysis of T_m data, and C. Young for help with analysis of NMR data. We also thank R. A. Collins and J. G. Omichinski for critical reading of the manuscript, C. Hoogstraten for the HCCH-E.COSY pulse sequence, and A. Majumdar for the HNN-COSY pulse sequences.

SUPPORTING INFORMATION AVAILABLE

Figure S1 shows the effect of $MgCl_2$ and $Co(NH_3)_6^{3+}$ on SL5; it includes overlays of the H6−C6/H8−C8 region of 2D $^1H-^{13}C$ CT-HSQC spectra of SL5 under various buffer conditions. Figure S2 shows 1D ^{31}P spectra of $SL5^{free}$ and $SL5^{Mg}$. Figure S3 shows UV denaturation profiles of SL5 under various salt and ionic strength conditions. Table S1 contains resonance assignments for $SL5^{Mg}$. Table S2 lists resolved SL5 protons that gave a NOE cross-peak to $Co(NH_3)_6^{3+}$ in ^{13}C-edited HMQC-NOESY spectra. Table S3 lists the results of the $MnCl_2$ titrations. Table S4 gives the statistics from the structure calculation of $SL5^{Mg}$ with modeling of $Mn(H_2O)_6^{2+}$. This material is available free of charge via the Internet at http://pubs.acs.org.

REFERENCES

1. Cate, J. H., and Doudna, J. A. (1996) Metal-binding sites in the major groove of a large ribozyme domain, *Structure 4*, 1221−1229.
2. Adams, P. L., Stahley, M. R., Kosek, A. B., Wang, J., and Strobel, S. A. (2004) Crystal structure of a self-splicing group I intron with both exons, *Nature 430*, 45−50.
3. Guo, F., Gooding, A. R., and Cech, T. R. (2004) Structure of the *Tetrahymena* ribozyme: Base triple sandwich and metal ion at the active site, *Mol. Cell 16*, 351−362.
4. Golden, B. L., Kim, H., and Chase, E. (2004) Crystal structure of a phage Twort group I ribozyme-product complex, *Nat. Struct. Mol. Biol. 12*, 82−88.
5. Correll, C. C., Freeborn, B., Moore, P. B., and Steitz, T. A. (1997) Metals, motifs, and recognition in the crystal structure of a 5S rRNA domain, *Cell 91*, 705−712.
6. Klein, D. J., Moore, P. B., and Steitz, T. A. (2004) The contribution of metal ions to the structural stability of the large ribosomal subunit, *RNA 10*, 1366−1379.
7. Fedor, M. J. (2002) The role of metal ions in RNA catalysis, *Curr. Opin. Struct. Biol. 12*, 289−295.
8. Stahley, M. R., and Strobel, S. A. (2005) Structural evidence for a two-metal-ion mechanism of group I intron splicing, *Science 309*, 1587−1590.
9. Draper, D. E. (2004) A guide to ions and RNA structure, *RNA 10*, 335−343.
10. Collins, R. A. (2002) The *Neurospora* Varkud satellite ribozyme, *Biochem. Soc. Trans. Rev. 30*, 1122−1126.
11. Lilley, D. M. (2004) The Varkud satellite ribozyme, *RNA 10*, 151−158.
12. Saville, B. J., and Collins, R. A. (1990) A site-specific self-cleavage reaction performed by a novel RNA in *Neurospora* mitochondria, *Cell 61*, 685−696.

13. Guo, H. C. T., and Collins, R. A. (1995) Efficient trans-cleavage of a stem-loop RNA substrate by a ribozyme derived from *Neurospora* VS RNA, *EMBO J. 14*, 368−376.
14. Andersen, A., and Collins, R. A. (2000) Rearrangement of a stable RNA secondary structure during VS ribozyme catalysis, *Mol. Cell 5*, 469−478.
15. Jones, F. D., Ryder, S. P., and Strobel, S. A. (2001) An efficient ligation reaction promoted by a Varkud satellite ribozyme with extended 5′- an 3′-termini, *Nucleic Acids Res. 29*, 5115−5120.
16. Lafontaine, D. A., Wilson, T. J., Norman, D. G., and Lilley, D. M. (2001) The A730 loop is an important component of the active site of the VS ribozyme, *J. Mol. Biol. 312*, 663−674.
17. Hiley, S. L., Sood, V. D., Fan, J., and Collins, R. A. (2002) 4-Thio-U cross-linking identifies the active site of the VS ribozyme, *EMBO J. 21*, 4691−4698.
18. Sood, V. D., Beattie, T. L., and Collins, R. A. (1998) Identification of phosphate groups involved in metal binding and tertiary interactions in the core of the *Neurospora* VS ribozyme, *J. Mol. Biol. 282*, 741−750.
19. Lafontaine, D. A., Norman, D. G., and Lilley, D. M. (2002) The global structure of the VS ribozyme, *EMBO J. 21*, 2461−2471.
20. Hiley, S. L., and Collins, R. A. (2001) Rapid formation of a solvent-inaccessible core in the *Neurospora* Varkud satellite ribozyme, *EMBO J. 20*, 5461−5469.
21. Flinders, J., and Dieckmann, T. (2001) A pH controlled conformational switch in the cleavage site of the VS ribozyme substrate RNA, *J. Mol. Biol. 308*, 665−679.
22. Michiels, P. J. A., Schouten, C. H. J., Hilbers, C. W., and Heus, H. A. (2000) Structure of the ribozyme substrate hairpin of *Neurospora* VS RNA: A close look at the cleavage site, *RNA 6*, 1821−1832.
23. Flinders, J., and Dieckmann, T. (2004) The solution structure of the VS ribozyme active site loop reveals a dynamic "hot-spot", *J. Mol. Biol. 341*, 935−949.
24. Hoffmann, B., Mitchell, G. T., Gendron, P., Major, F., Andersen, A. A., Collins, R. A., and Legault, P. (2003) NMR structure of the active conformation of the Varkud satellite ribozyme cleavage site, *Proc. Natl. Acad. Sci. U.S.A. 100*, 7003−7008.
25. Campbell, D. O., and Legault, P. (2005) NMR structure of the Varkud satellite ribozyme stem-loop V RNA and magnesium-ion binding from chemical-shift mapping, *Biochemistry 44*, 4157−4170.
26. Rastogi, T., Beattie, T. L., Olive, J. E., and Collins, R. A. (1996) A long-range pseudoknot is required for activity of the *Neurospora* VS ribozyme, *EMBO J. 15*, 2820−2825.
27. Andersen, A. A., and Collins, R. A. (2001) Intramolecular secondary structure rearrangement by the kissing interaction of the *Neurospora* VS ribozyme, *Proc. Natl. Acad. Sci. U.S.A. 98*, 7730−7735.
28. Collins, R. A., and Olive, J. E. (1993) Reaction conditions and kinetics of self-cleavage of a ribozyme derived from *Neurospora* VS RNA, *Biochemistry 32*, 2795−2799.
29. Murray, J. B., Seyhan, A. A., Walter, N. G., Burke, J. M., and Scott, W. G. (1998) The hammerhead, hairpin and VS ribozymes are catalytically proficient in monovalent cations alone, *Chem. Biol. 5*, 587−595.
30. Maguire, J. L., and Collins, R. A. (2001) Effects of cobalt hexammine on folding and self-cleavage of the *Neurospora* VS ribozyme, *J. Mol. Biol. 309*, 45−56.
31. Sood, V. D., Yekta, S., and Collins, R. A. (2002) The contribution of 2′-hydroxyls to the cleavage activity of the *Neurospora* VS ribozyme, *Nucleic Acids Res. 30*, 1132−1138.
32. Quigley, G. J., and Rich, A. (1976) Structural domains of transfer RNA molecules, *Science 194*, 796−806.
33. Pley, H. W., Flaherty, K. M., and McKay, D. B. (1994) Three-dimensional structure of a hammerhead ribozyme, *Nature 372*, 68−74.
34. Puglisi, E. V., and Puglisi, J. D. (1998) HIV-1 A-rich RNA loop mimics the tRNA anticodon structure, *Nat. Struct. Biol. 5*, 1033−1036.
35. Lebars, I., Yoshizawa, S., Stenholm, A. R., Guittet, E., Douthwaite, S., and Fourmy, D. (2003) Structure of 23S rRNA hairpin 35 and its interaction with the tylosin-resistance methyltransferase RlmAII, *EMBO J. 22*, 183−192.
36. Stallings, S. C., and Moore, P. B. (1997) The structure of an essential splicing element: Stem loop IIa from yeast U2 snRNA, *Structure 5*, 1173−1185.
37. Gutell, R. R., Cannone, J. J., Konings, D., and Gautheret, D. (2000) Predicting U-turns in ribosomal RNA with comparative sequence analysis, *J. Mol. Biol. 300*, 791−803.
38. Franch, T., and Gerdes, K. (2000) U-Turns and regulatory RNAs, *Curr. Opin. Microbiol. 3*, 159−164.
39. Ashraf, S. S., Ansari, G., Guenther, R., Sochacka, E., Malkiewicz, A., and Agris, P. F. (1999) The uridine in "U-turn": Contributions to tRNA-ribosomal binding, *RNA 5*, 503−511.
40. Vuister, G. W., and Bax, A. (1992) Resolution enhancement and spectral editing of uniformly ^{13}C-enriched proteins by homonuclear broadband ^{13}C decoupling, *J. Magn. Reson. 98*, 428−435.
41. Santoro, J., and King, G. C. (1992) A constant-time 2D overbodenhausen experiment for inverse correlation of isotopically enriched species, *J. Magn. Reson. 97*, 202−207.
42. Pardi, A., and Nikonowicz, E. P. (1992) Simple procedure for resonance assignment of the sugar protons in ^{13}C-labeled RNAs, *J. Am. Chem. Soc. 114*, 9202−9203.
43. Ikura, M., Kay, L. E., Tschudin, R., and Bax, A. (1990) Three-dimensional NOESY-HMQC spectroscopy of a ^{13}C-labeled protein, *J. Magn. Reson. 86*, 204−209.
44. Kay, L. E., Keifer, P., and Saarinen, T. (1992) Pure absorption gradient enhanced heteronuclear single quantum correlation spectroscopy with improved sensitivity, *J. Am. Chem. Soc. 114*, 10663−10665.
45. Mueller, L., Legault, P., and Pardi, A. (1995) Improved RNA structure determination by detection of NOE contacts to exchange-broadened amino groups, *J. Am. Chem. Soc. 117*, 11043−11048.
46. Skleñár, V., Peterson, R. D., Rejante, M. R., and Feigon, J. (1994) Correlation of nucleotide base and sugar protons in a ^{15}N-labeled HIV-1 RNA oligonucleotide by ^{1}H-^{15}N HSQC experiments, *J. Biomol. NMR 4*, 117−122.
47. Skleñár, V., Miyashiro, H., Zon, G., Miles, H. T., and Bax, A. (1986) Assignment of the ^{31}P and ^{1}H resonances in oligonucleotides by two-dimensional NMR spectroscopy, *FEBS Lett. 208*, 94−98.
48. Dingley, A. J., and Grzesiek, S. (1998) Direct observation of hydrogen bonds in nucleic acid base pairs by internucleotide $^{2}J_{NN}$ couplings, *J. Am. Chem. Soc. 120*, 8293−8297.
49. Hennig, M., and Williamson, J. R. (2000) Detection of NH·N hydrogen bonding in RNA via scalar couplings in the absence of observable imino proton resonances, *Nucleic Acids Res. 28*, 1585−1593.
50. Schwalbe, H., Marino, J. P., King, G. C., Wechselberger, P., Bermel, W., and Griesinger, C. (1994) Determination of a complete set of coupling constants in ^{13}C-labeled oligonucleotides, *J. Biomol. NMR 4*, 631−644.
51. Delaglio, F., Grzesiek, S., Vuister, G. W., Zhu, G., Pfeifer, J., and Bax, A. (1995) NMRPipe: A multidimensional spectral processing system based on UNIX pipes, *J. Biomol. NMR 6*, 277−293.
52. Johnson, B. A., and Blevins, R. A. (1994) NMRView: A computer program for the visualization and analysis of NMR data, *J. Biomol. NMR 4*, 603−614.
53. Wishart, D. S., Bigam, C. G., Yao, J., Dyson, H. J., Oldfield, E., Markley, J. L., and Sykes, B. D. (1995) ^{1}H, ^{13}C, ^{15}N chemical shift referencing in biomolecular NMR, *J. Biomol. NMR 6*, 135−140.
54. Wijmenga, S. S., Mooren, M. M. W., and Hilbers, C. W. (1993) NMR of nucleic acids; from spectrum to structure, in *NMR of macromolecules: A practical approach* (Roberts, G. C. K., Ed.) pp 217−288, Oxford University Press, New York.
55. Brünger, A. T. (1992) *X-PLOR 3.1 Manual*, Yale University Press, New Haven, CT.
56. Schwieters, C. D., Kuszewski, J. J., Tjandra, N., and Clore, G. M. (2003) The Xplor-NIH NMR molecular structure determination package, *J. Magn. Reson. 160*, 66−74.
57. Koradi, R., Billeter, M., and Wüthrich, K. (1996) MOLMOL: A program for display and analysis of macromolecular structures, *J. Mol. Graphics 14*, 51−55.
58. Pascal, S. M., Muhandiram, D. R., Yamazaki, T., Forman-Kay, J. D., and Kay, L. E. (1994) Simultaneous acquisition of ^{15}N and ^{13}C-edited NOE spectra of proteins dissolved in H_2O, *J. Magn. Reson., Ser. B 103*, 197−201.
59. Kleywegt, G. T., and Jones, T. A. (1998) Databases in protein crystallography, *Acta Crystallogr. D54*, 1119−1131.
60. Milligan, J. F., Groebe, D. R., Witherell, G. W., and Uhlenbeck, O. C. (1987) Oligoribonucleotide synthesis using T7 RNA polymerase and synthetic DNA templates, *Nucleic Acids Res. 15*, 8783−8798.

61. Beattie, T. L., Olive, J. E., and Collins, R. A. (1995) A secondary-structure model for the self-cleaving region of *Neurospora* VS RNA, *Proc. Natl. Acad. Sci. U.S.A. 92*, 4686−4690.
62. Clore, G. M., Gronenborn, A. M., Piper, E. A., McLaughlin, L. W., Graeser, E., and Van Boom, J. H. (1984) The solution structure of a RNA pentadecamer comprising the anticodon loop and stem of yeast tRNAPhe, *Biochem. J. 221*, 737−751.
63. Schweisguth, D. C., and Moore, P. B. (1997) On the conformation of the anticodon loops of initiator and elongator methionine tRNAs, *J. Mol. Biol. 267*, 505−519.
64. Sundaram, M., Durant, P. C., and Davis, D. R. (2000) Hypermodified nucleosides in the anticodon of $tRNA^{Lys}$ stabilize a canonical U-turn structure, *Biochemistry 39*, 12575−12584.
65. Cabello-Villegas, J., Tworowska, I., and Nikonowicz, E. P. (2004) Metal ion stabilization of the U-turn of the A_{37} N^6-dimethylallyl-modified anticodon stem-loop of *Escherichia coli* $tRNA^{Phe}$, *Biochemistry 43*, 55−66.
66. Jucker, F. M., and Pardi, A. (1995) GNRA tetraloops make a U-turn, *RNA 1*, 219−222.
67. Legault, P., and Pardi, A. (1994) ^{31}P chemical shift as a probe of structural motifs in RNA, *J. Magn. Reson., Ser. B 103*, 82−86.
68. Feig, A. L. (2000) The use of manganese as a probe for elucidating the role of magnesium ions in ribozymes, *Met. Ions Biol. Syst. 37*, 157−182.
69. Gonzalez, R. L., Jr., and Tinoco, I., Jr. (2001) Identification and characterization of metal ion binding sites in RNA, *Methods Enzymol. 338*, 421−443.
70. Cowan, J. A. (1993) Metallobiochemistry of RNA. $Co(NH_3)_6^{3+}$ as a probe for Mg^{2+}(aq) binding sites, *J. Inorg. Biochem. 49*, 171−175.
71. Juneau, K., Podell, E., Harrington, D. J., and Cech, T. R. (2001) Structural basis for the enhanced stability of a mutant ribozyme domain and a detailed view of RNA-solvent interactions, *Structure 9*, 221−231.
72. Misra, V. K., and Draper, D. E. (1999) On the role of magnesium ions in RNA stability, *Biopolymers 48*, 113−135.
73. Gonzalez, R. L., Jr., and Tinoco, I., Jr. (1999) Solution structure and thermodynamics of a divalent metal ion binding site in an RNA pseudoknot, *J. Mol. Biol. 289*, 1267−1282.
74. Colmenarejo, G., and Tinoco, I., Jr. (1999) Structure and thermodynamics of metal binding in the P5 helix of a group I intron ribozyme, *J. Mol. Biol. 290*, 119−135.
75. Butcher, S. E., Allain, F. H.-T., and Feigon, J. (2000) Determination of metal ion binding sites within the hairpin ribozyme domains by NMR, *Biochemistry 39*, 2174−2182.
76. Bertini, I., and Lychinat, C. (1986) *NMR of paramagnetic molecules in biological systems*, Benjamin/Cummings, Menlo Park, CA.
77. Ogle, J. M., Brodersen, D. E., Clemons, W. M., Jr., Tarry, M. J., Carter, A. P., and Ramakrishanan, V. (2001) Recognition of cognate transfer RNA by the 30S ribosomal subunit, *Science 292*, 897−902.
78. Silvian, L. F., Wang, J., and Steitz, T. A. (1999) Insights into editing from an ile-tRNA synthetase structure with $tRNA^{ile}$ and mupirocin, *Science 292*, 897−902.
79. Tzokov, S. B., Murray, I. A., and Grasby, J. A. (2002) The role of magnesium ions and 2′-hydroxyl groups in the VS ribozyme-substrate interaction, *J. Mol. Biol. 324*, 215−226.

BI0607150